ACS OMEGA

http://pubs.acs.org/journal/acsodf

Article

Trace Doping of $Pb(OH)_2$ Species on PdPb Alloys Boost Highly Active and Stable Ethanol Oxidation

Jialu Huang, Zhiming Ni, Xiaofan Song, Han Li, Xiaolei Chen, Aichuang Zhang, Hu Yang, Yuan Liu,* Peng Zhu, Ping Hua,* and Xiaolei Yuan*

Cite This: *ACS Omega* 2022, 7, 35720−35726

Read Online

ACCESS | Metrics & More | Article Recommendations | Supporting Information

ABSTRACT: PdPb nanocrystals have drawn considerable attention due to their excellent catalytic properties, while their practical applications have been impeded by the severe degradation of activity, which is caused by the adsorption of intermediates (especially CO) during the operation. Herein, we first present porous PdPb alloys with the incorporation of amorphous $Pb(OH)_2$ species as highly active and stable electrocatalysts. Alloying Pd with Pb species is initially proposed to optimize the Pd−Pd interatomic distance and adjust the d-band center of Pd. Importantly, the amorphous $Pb(OH)_2$ species are beneficial to promoting the formation of OH_{ad} and the removal of CO_{ad}. Therefore, PdPb-$Pb(OH)_2$ catalysts show a mass activity of 3.18 A mg_{Pd}^{-1} and keep excellent stability for the ethanol oxidation reaction (EOR). In addition, further CO stripping and a series of CO poisoning experiments indicate that PdPb-$Pb(OH)_2$ composites possess much better CO tolerance benefiting from the tuned electronic structure of Pd and surface incorporation of $Pb(OH)_2$ species.

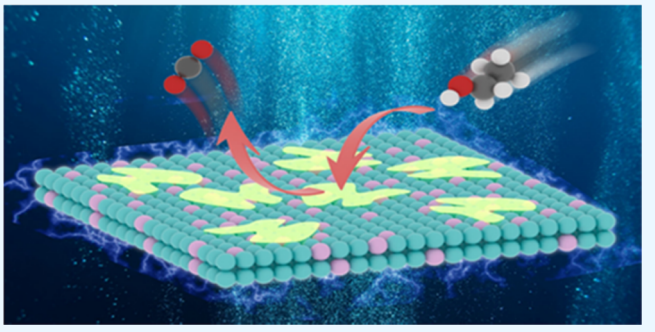

1. INTRODUCTION

Direct ethanol fuel cells (DEFCs) have drawn increasing attention due to their unique properties of ethanol fuel, including high power density, low toxicity, and convenient storage.[1,2] Despite the great progress achieved in the past few decades, DEFCs have not yet achieved widespread commercial applications, which might be due to the high cost and low operating durability of electrocatalysts.[3] Among the electrocatalysts for DEFCs, platinum (Pt)-based catalysts have been widely investigated owing to their geometric and electronic modifications, while the high cost and poor durability have limited their practical applications.[4] Therefore, how to use less Pt or even develop non-Pt-based catalysts with advanced performance for the ethanol oxidation reaction (EOR) is essential.

It is well known that palladium (Pd) has a higher catalytic activity for the EOR in alkaline medium.[5] However, the practical applications of Pd-based catalysts have been hindered by the relatively low activity and severe degradation of activity, which is caused by the adsorption of CO intermediate during the operation.[6] To overcome the above issues, a series of bimetallic Pd−M catalysts (M = Ag,[7] Bi,[8] Ni,[9] Pb,[10] etc.) have been successfully developed based on the adjustment of their d-band center. With regard to this, bimetallic PdPb catalysts have received considerable attention. For example, Guo et al. reported bimetallic PdPb nanowires that have a defect-rich and stable structure.[11] They demonstrated that ultrathin PdPb nanowires (PdPb NWs) can exhibit an activity as high as 6.3 times that of commercial Pd/C due to the synergistic effect. Furthermore, with the introduction of Pb, Cabot and his coworkers synthesized intermetallic Pd_3Pb nanocrystals with controlled size and cubic geometry exposing (100) facets, which show high EOR activity and stability.[12] Despite the success, the design of most PdPb catalysts for the EOR is concerned with alloys and their structure. In contrast, utilizing the synergy between Pd and metal hydroxides can accelerate the dissociation of H_2O to generate the absorbed hydroxide species (OH_{ad}) near the Pd active sites, which favor the oxidative removal of the absorbed CO species (CO_{ad}) and boost EOR performance. Li's group first assembled Pd-based hybrids using defective $Ni(OH)_2$ nanoflakes as supports, which can dramatically improve the EOR performance in an alkaline solution.[13] Moreover, amorphous $Bi(OH)_3$ has been reported to modify the Pd nanocrystals with well-defined morphologies.[14,15] The surface modification of $Bi(OH)_3$ was proved to promote the formation of OH_{ad}, which can promote the removal of CO intermediate, leading to a superior EOR

Received: June 14, 2022
Accepted: September 21, 2022
Published: September 28, 2022

https://doi.org/10.1021/acsomega.2c03693
ACS Omega 2022, 7, 35720−35726

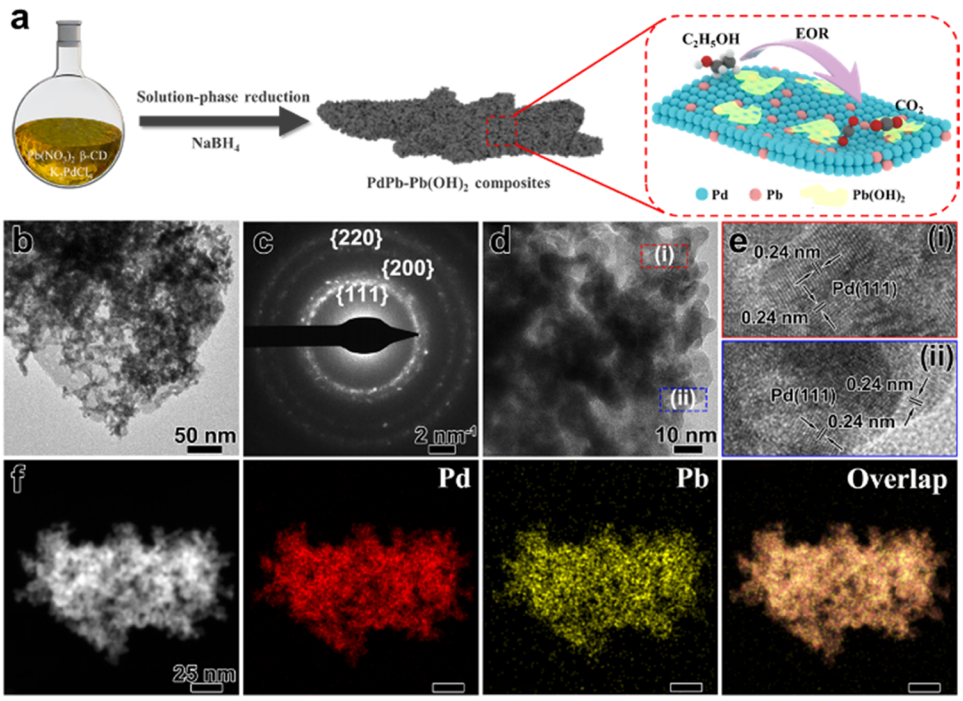

Figure 1. (a) Schematic illustration of the PdPb-$Pb(OH)_2$ composite forming process. (b) TEM, (c) SAED, (d, e) HRTEM images, and (f) EDS mapping of PdPb-$Pb(OH)_2$ composites.

stability. However, much less attention has been paid to the synergy between Pd and Pb hydroxides, especially the integration of amorphous Pb hydroxides in the PdPb system.

Herein, we have successfully developed porous PdPb nanocrystals with the modification of amorphous $Pb(OH)_2$ using a solution-phase method. The catalyst arrangement is initially proposed by alloying Pd with Pb species, and the incorporation of Pb species can increase the orbital overlap between the Pd surface and Pb, which could widen the metal d-band of Pd and then cause its d-band to shift down, thus leading to the weaker adsorption of CO. In addition, the porous structure with the large surface area is beneficial to high utilization efficiency of Pd, which further contributes to the enhancement of EOR activity. More importantly, the amorphous $Pb(OH)_2$ can promote the formation of OH_{ad} and the removal of CO_{ad}. Therefore, the as-prepared PdPb-$Pb(OH)_2$ catalysts show a mass activity of 3.18 A mg_{Pd}^{-1}, which is 2.5 times higher than that of commercial Pd/C. Interestingly, there is no notable decline in EOR activity during five successive cycles (50,000 s). At the same time, PdPb-$Pb(OH)_2$ catalysts exhibit a superior tolerance to CO intermediate as demonstrated by a series of CO antitoxicity experiments. Based on the above, this work emphasizes the significance of a bimetallic PdPb structure and its synergy with Pb hydroxides.

2. EXPERIMENTAL SECTION

2.1. Chemicals. Commercial Pd/C (10 wt % of Pd), potassium tetrachloropalladate (K_2PdCl_4, 99.95%), and β-cyclodextrins ($C_{42}H_{70}O_{35}$, 98%) were purchased from Aladdin. Lead nitrate ($Pb(NO_3)_2$, 99%) was obtained from Yonghua Chemical. Ethylene glycol ($C_2H_6O_2$, 98%) was purchased from Macklin. Sodium borohydride ($NaBH_4$, 96%) was obtained from Enox. Nafion perfluorinated resin solution (5 wt %) was obtained from Alfa Aesar. All chemicals were used as received without further purification.

2.2. Synthesis of Porous PdPb-$Pb(OH)_2$ Composites. In a typical synthesis, β-cyclodextrin aqueous solution was obtained by adding β-cyclodextrin (2.27 g, 10 Mm) into 200 mL of deionized water and then ultrasonicated for 30 min. Next, $Pb(NO_3)_2$ was dissolved in a mixture aqueous solution, containing 2 mL of ethylene glycol and 8 mL of β-cyclodextrin. Moreover, K_2PdCl_4 was added to 2 mL of β-cyclodextrin aqueous solution. The above K_2PdCl_4 solution and $Pb(NO_3)_2$ solution were then mixed with 183 mL of β-cyclodextrin aqueous solution to produce the yellow clear solution (the molar ratio of Pd^{2+} to Pb^{2+} was 3:1). Five milliliters of a newly prepared 40 mM $NaBH_4$ in β-cyclodextrin aqueous solution was quickly injected into the aforesaid yellow clear solution under stirring conditions. The resultant mixture was kept at room temperature for 7 days to verify the completed reaction. The black products were collected and then washed three times using the ethanol and acetone mixture (1:1). The porous PdPb-$Pb(OH)_2$ composites were finally obtained by freeze-drying. To obtain the different ratios of Pd/Pb products, we adjusted the feeding molar ratios of Pd/Pb precursors as 1:1 and 1:3, respectively.

2.3. Characterization. To characterize the nanocrystal structure, X-ray diffraction (XRD) was carried out on an Ultima IV multipurpose X-ray diffractometer with Cu Kα radiation (λ = 1.5406 Å). X-ray photoelectron spectroscopy (XPS) tests were conducted on a Kratos AXIS Untraded ultrahigh vacuum (UHV) surface analysis system, and C 1s (284.8 eV) was used to calibrate the binding energy. To investigate the morphology of the as-obtained products, scanning electron microscopy (SEM) images were obtained at 5 kV using a Gemini SEM 300 from Carl Zeiss. Transmission electron microscopy (TEM) was carried out on a TECNAI G2 LaB6 at 200 kV, and the energy-dispersive X-ray spectroscopy (EDS) mapping was obtained on a

https://doi.org/10.1021/acsomega.2c03693
ACS Omega 2022, 7, 35720−35726

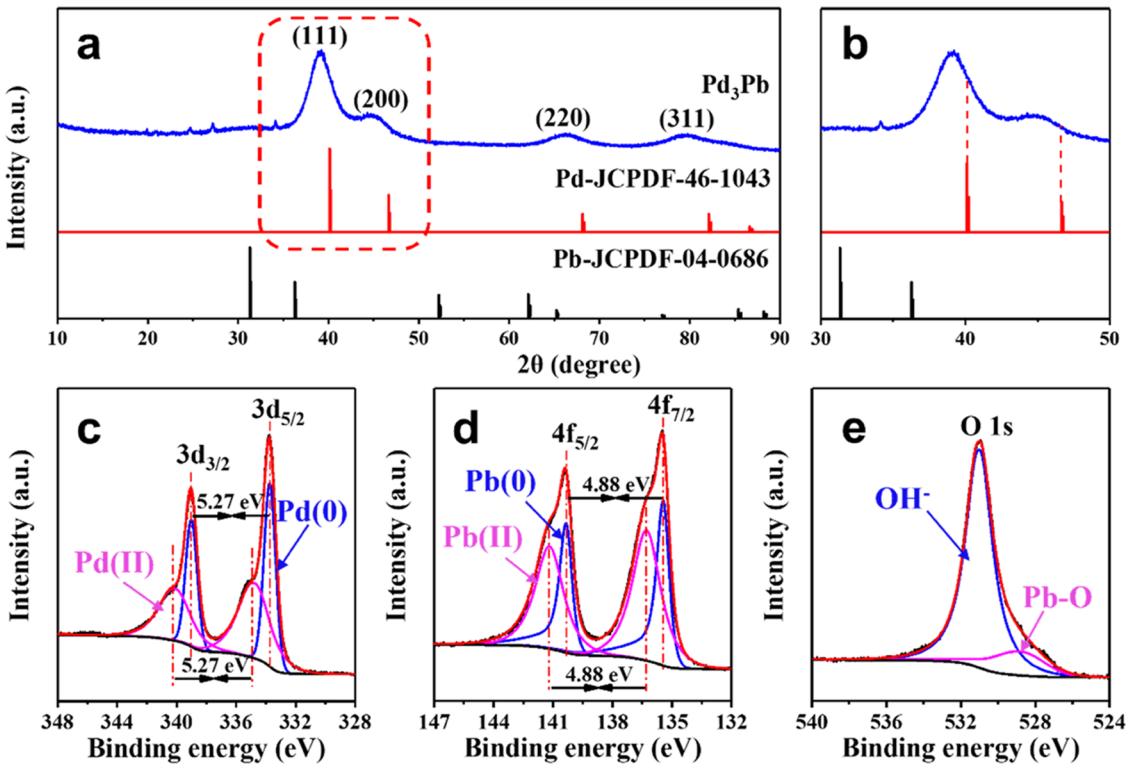

Figure 2. (a) XRD pattern of the as-prepared PdPb-$Pb(OH)_2$ composites. (b) Enlarged image of the red region. XPS spectra: (c) Pd 3d, (d) Pb 4f, and (e) O 1s.

TECNAI G2F20 at 200 kV. To identify the composition of the products, inductively coupled plasma atomic emission spectroscopy (ICP-AES) was performed on a Varian 710-ES. A nitrogen gas adsorption/desorption analyzer (MicroActive for ASAP 2460) was employed at 77 K to measure the pore volume (V_p), pore size (D_p), and Brunauer−Emmett−Teller (BET) specific surface area (S_{BET}) of PdPb-$Pb(OH)_2$ composites. The Barrett−Joyner−Halenda (BJH) model with the Halsey equation was used to analyze the adsorption and desorption data and yield pore size distribution.

2.4. Electrochemical Measurements. A standard three-electrode system was used to carry out all of the electrochemical experiments on a CHI660E workstation. A glassy carbon electrode (3 mm in diameter), Pt gauze, and saturated calomel electrode (SCE) were employed as the working, counter, and reference electrodes, respectively. To obtain a homogeneous ink, the as-prepared catalysts and Vulcan XC-72 carbon (20 wt % of the catalysts) were dispersed in 1 mL of Nafion solution, ethanol, and water (the volume ratio was 0.6:1:1) and ultrasonicated for 30 min. The ink solution was drop-cast onto the glassy carbon electrode and then dried at room temperature. The Pd loading for all of the catalysts was kept at 28 μg cm^{-2}, and the amount of the catalysts was controlled based on ICP-AES measurements.

Cyclic voltammetry (CV) curves were plotted at a scan rate of 50 mV s^{-1} in a N_2-saturated 1 M NaOH and 1 M NaOH + 1 M ethanol solution. The chronoamperometric (CA) measurements were performed at −0.2 V (vs SCE) in the N_2-saturated 1 M NaOH and 1 M ethanol solution. In addition, CO stripping experiments were carried out in 1 M NaOH solution. High-purity gaseous CO was bubbled into the electrolyte at the potential of −0.86 V (vs SCE) for 30 min. Subsequently, to remove the dissolved CO in the solution, gaseous N_2 was bubbled into the above electrolyte for 15 min. Finally, two complete cycles of CO-stripping CV curves were obtained at a scan rate of 50 mV s^{-1}. Furthermore, gaseous CO was purged into the 1 M NaOH + 1 M ethanol solution at 200 s during the CA test to simulate the intermediate products.

3. RESULTS AND DISCUSSION

In this work, PdPb-$Pb(OH)_2$ composites were successfully prepared by a solution-phase chemical approach (Figure 1a).[16] Potassium tetrachloropalladate (K_2PdCl_4) and lead nitrate ($Pb(NO_3)_2$) as precursors and β-cyclodextrin as a surfactant were first dissolved in deionized water. The mixture solution was reacted with sodium borohydride ($NaBH_4$), and the resultant mixture was then maintained at room temperature for 7 days to verify the completed reaction. The CV process could oxidize metallic Pb to PbO in a basic solution. The formation of PbO will exist as insoluble $Pb(OH)_2$ when the potential reached above 0.54 V (vs the reversible hydrogen electrode (RHE)). The morphology of PdPb-$Pb(OH)_2$ composites was examined by SEM and TEM, as shown in Figures 1b and S1. Both SEM and TEM images exhibit that PdPb-$Pb(OH)_2$ composites with the porous structure are successfully synthesized. As seen from Figure 1c, the selected area electron diffraction (SAED) results reveal a polycrystalline nature of PdPb-$Pb(OH)_2$ composites with the {111}, {200}, and {220} facets of Pd.[17] Furthermore, as shown in Figures 1d,e and S2, high-resolution TEM (HRTEM) image shows that the lattice distance is 0.24 nm, which corresponds to the Pd(111) facet. The lattice spacing and crystal structure of $Pb(OH)_2$ species cannot be observed, suggesting that $Pb(OH)_2$ species belong to an amorphous structure. Importantly, EDS elemental mapping was used to explore the distribution of Pd and Pb in the nanocrystals. As shown in Figure 1f, both Pd and Pb are

https://doi.org/10.1021/acsomega.2c03693
ACS Omega 2022, 7, 35720−35726

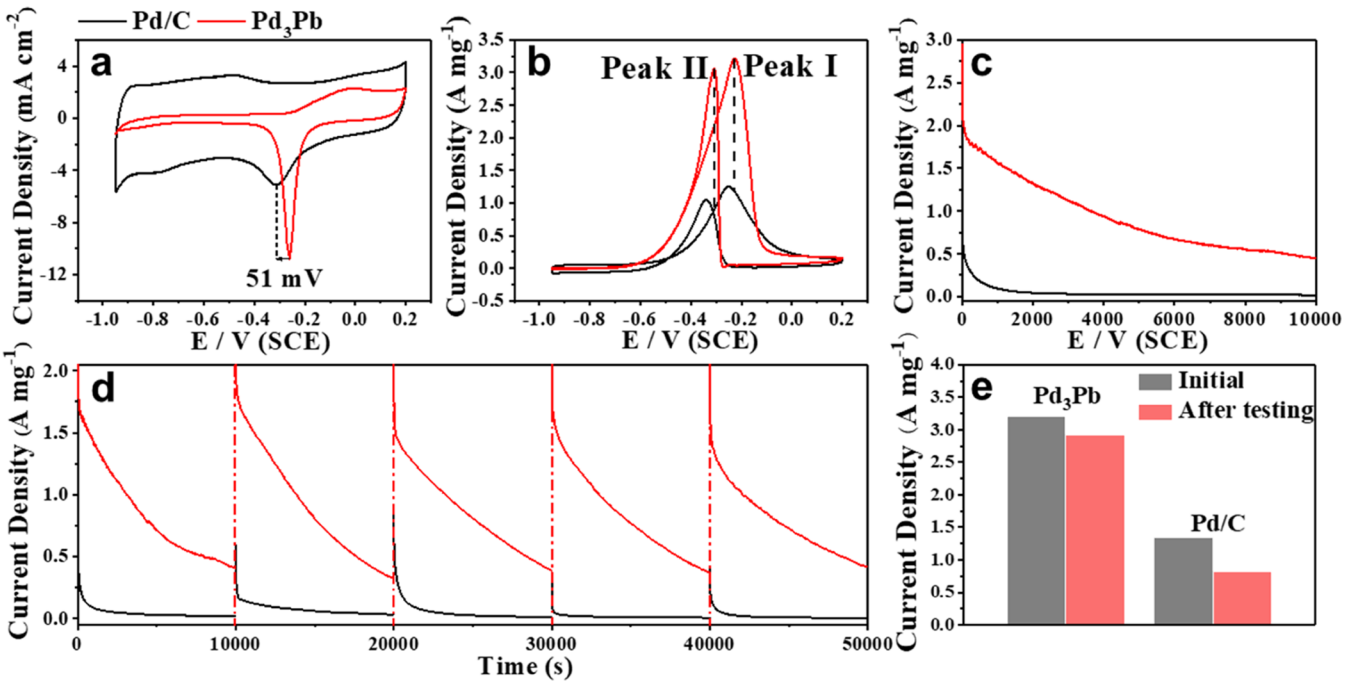

Figure 3. CV curves of PdPb-$Pb(OH)_2$ composites and commercial Pd/C measured in N_2-saturated (a) 1 M NaOH and (b) 1 M NaOH + 1 M ethanol at a scan rate of 50 mV s^{-1}. (c, d) CA curves in the N_2-saturated 1 M NaOH + 1 M ethanol solution recorded at −0.2 V. (e) Histogram showing the mass activity before and after the stability test.

uniformly distributed in the nanocrystals, meaning that PdPb-$Pb(OH)_2$ composites may have a bimetallic structure. Besides, the mass ratio of Pd/Pb is 70.95:29.05 by EDS quantification (Figure S3).

To investigate the crystal structure of PdPb-$Pb(OH)_2$ composites, XRD was employed to test the as-prepared products. As illustrated in Figure 2a, the diffraction peaks at 39.1, 44.9, 66.3, and 79,3° can be indexed to the (111), (200), (220), and (311) crystal planes of face-centered cubic Pd (JCPDF no. 46-1043), respectively.[18,19] Additionally, no peaks can be in line with $Pb(OH)_2$, further indicating that $Pb(OH)_2$ is an amorphous structure. Importantly, Figure 2b shows that the peak position of PdPb-$Pb(OH)_2$ composites shifts to the lower angles compared to pure Pd, indicating that the larger sized Pb atoms are doped into the lattice of Pd. In addition, to investigate the specific surface area and pore size distribution, BET experiments were performed on both PdPb-$Pb(OH)_2$ composites. Based on the BET results, PdPb-$Pb(OH)_2$ composites possess a large specific surface area, as shown in Figure S4 and Table S1. The compositions and chemical states of Pd and Pb elements were characterized by XPS. As shown in Figure 2c, two asymmetric peaks can be observed, which can be ascribed to Pd $3d_{3/2}$ and $3d_{5/2}$ orbitals, respectively.[20,21] The peaks at 339.02 and 333.74 eV can be assigned to metallic Pd(0), while the peaks at 340.09 and 334.76 eV can be indexed to Pd(II). Figure 2d indicates two sets of peaks at the Pb 4f orbital, including $4f_{5/2}$ and $4f_{7/2}$ orbitals of Pb(0) and Pb(II).[22] In addition, the O 1s spectrum shows the weak peak of Pb−O at 528.81 eV and the prominent peak of OH^- at 530.98 eV (Figure 2e). As a result, both XRD and XPS results demonstrate that PdPb-$Pb(OH)_2$ composites possess two components, containing PdPb alloys and amorphous $Pb(OH)_2$ species.

According to the previous reports, the compositions of catalysts usually determine their electrocatalytic properties. To obtain higher catalytic performance, PdPb-$Pb(OH)_2$ composites were investigated by varying the feeding ratios of Pd and Pb precursors. Figure S5 exhibits that there is no big difference in the morphology and structure of PdPb-$Pb(OH)_2$ when the proportion of Pd/Pb ratios changes. As shown in Figure S6, the values obtained from the EDS quantification of PdPb-$Pb(OH)_2$ composites with the feeding ratios of 1:1 and 1:3 can match with their initial feeding ratios. Moreover, XPS measurements also indicate that PdPb-$Pb(OH)_2$ composites are made up of bimetallic PdPb alloys and $Pb(OH)_2$ (Figure S7). To obtain better catalytic performance, CV curves were carried out in the N_2-saturated 1 M NaOH and 1 M NaOH + 1 M ethanol solution (Figure S8). For the EOR, the mass activity of the porous composites with the feeding ratio of 3:1 is 3.18 A mg_{Pd}^{-1}, and its current density can maintain >0.45 A mg_{Pd}^{-1} after 10,000 s test, which is higher than those samples with different feeding ratios of Pd/Pb. As a result, this work will then focus on the investigation of PdPb-$Pb(OH)_2$ composites with a feeding ratio of 3:1.

To evaluate the electrochemical performance, both PdPb-$Pb(OH)_2$ and commercial Pd/C were carried out in the alkaline medium. As can be seen from Figure 3a, CV curves are first recorded in the N_2-saturated 1 M NaOH solution. The hydrogen adsorption/desorption peaks occur from −0.9 to −0.7 V on the Pd/C electrode, while the pronounced cathodic peak in the voltage range of −0.5 to −0.2 V belongs to the reduction of PdO to Pd and Pb^{2+} to Pb.[23] In contrast, there are no significant hydrogen adsorption/desorption peaks on the PdPb-$Pb(OH)_2$ electrode, indicating a high coverage of Pb species on the surface of Pd and the strong interaction between Pd and Pb species. Meanwhile, the anodic peak of PdPb-$Pb(OH)_2$ around 0 V can be ascribed to the formation of PdO and Pb^{2+}.[24,25] In addition, the location of the cathodic peak shows a slight positive shift on the PdPb-$Pb(OH)_2$ electrode compared to Pd/C, which suggests that the incorporation of

https://doi.org/10.1021/acsomega.2c03693
ACS Omega 2022, 7, 35720−35726

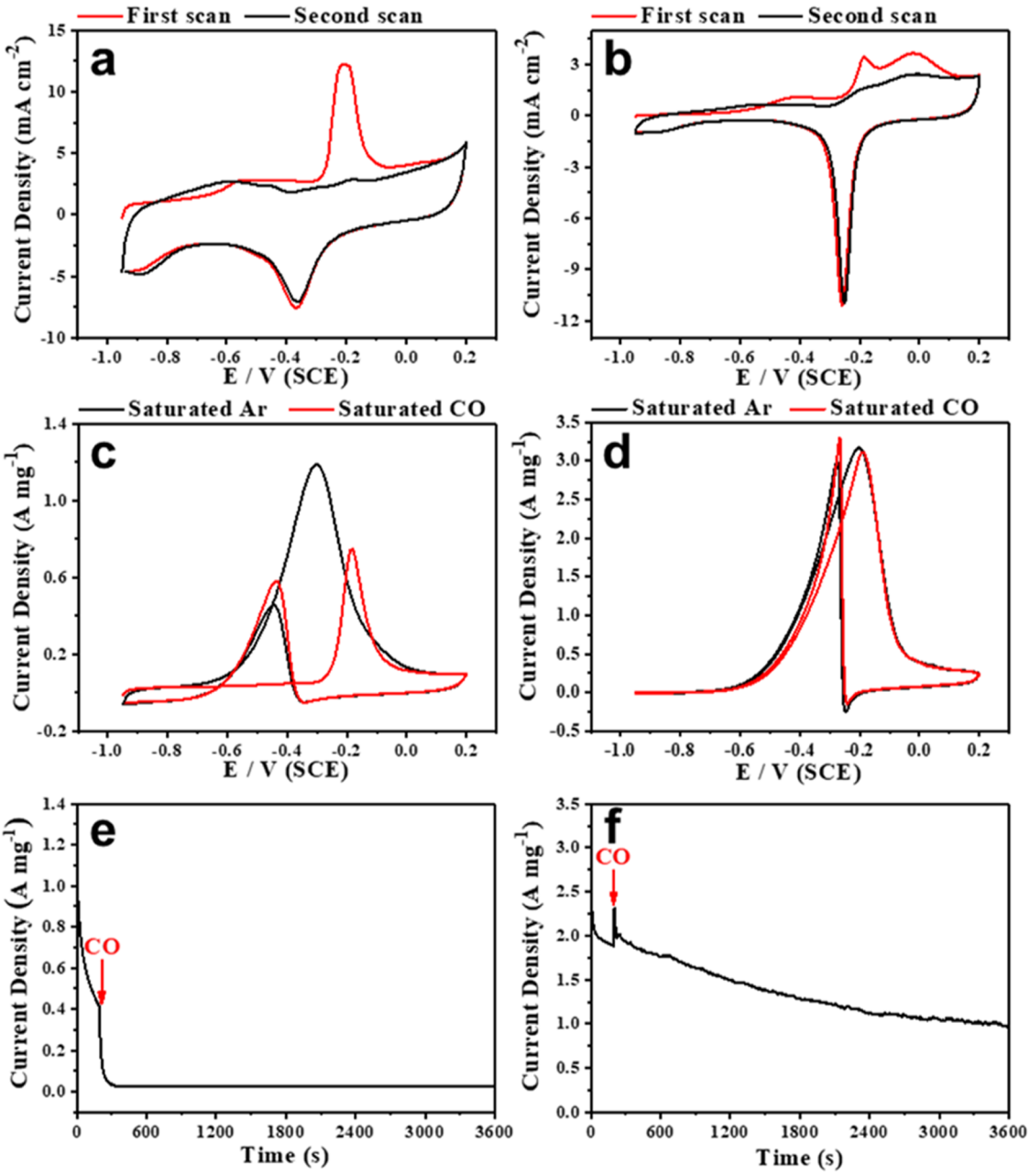

Figure 4. CO stripping measurements of (a) commercial Pd/C and (b) PdPb-Pb$(OH)_2$ composites. CV curves in N_2- or CO-saturated 1 M NaOH + 1 M ethanol solution of (c) commercial Pd/C and (d) PdPb-Pb$(OH)_2$ composites. Response of (e) commercial Pd/C and (f) PdPb-Pb$(OH)_2$ composites to bubbling CO in 1 M NaOH + 1 M ethanol during the CA tests.

Pb species can optimize the Pd−Pd interatomic distance and downshift the d-band center of Pd (Figure S9). In addition, it can also be seen that the modification of amorphous Pb$(OH)_2$ may accelerate the desorption of OH_{ad} species and oxidative removal of CO_{ad}.[14]

The EOR performance of PdPb-Pb$(OH)_2$ composites, pure Pd, and Pd/C was measured in the N_2-saturated 1 M NaOH + 1 M C_2H_5OH solution. Figures 3b and S10a illustrate that peak I between −0.4 and −0.1 V in the forward scan belongs to the oxidation of ethanol to intermediates, while peak II between −0.6 and −0.3 V in the reverse scan could be assigned to the further oxidation of intermediate products.[26] Therefore, the mass activity of PdPb-Pb$(OH)_2$ composites (3.18 A mg_{Pd}^{-1}) is 2.5 times higher than that of pure Pd (1.28 A mg_{Pd}^{-1}) and Pd/C (1.27 A mg_{Pd}^{-1}). To evaluate the EOR stability of PdPb-Pb$(OH)_2$ composites, CA tests were performed at the potential of −0.2 V. As shown in Figures 3c and S10b, the current density of pure Pd and Pd/C rapidly drops to nearly zero within 1000 s, suggesting unstable EOR performance. In contrast, the current density of PdPb-Pb$(OH)_2$ composites can remain around 0.4 A mg_{Pd}^{-1} after each cycle, showing the key role of the amorphous Pb$(OH)_2$ adjacent to the Pd active sites. As a result, PdPb-Pb$(OH)_2$ composites show better EOR performance compared to pure Pd and commercial Pd/C.

More impressively, the current density of PdPb-Pb$(OH)_2$ composites can be regained in a fresh electrolyte (Figure 3d). This is because PdPb-Pb$(OH)_2$ composites can be reactivated by several CV cycles in 1 M NaOH solution after each 10,000 s stability test, and then, the CA test was performed in a fresh 1

https://doi.org/10.1021/acsomega.2c03693
ACS Omega 2022, 7, 35720−35726

M NaOH + 1 M ethanol solution. After reactivation, there is no significant decrease in EOR activity over five consecutive cycles, further demonstrating the excellent EOR stability. After five consecutive cycles, Figure S11a depicts the well-maintained morphology of PdPb-Pb$(OH)_2$ composites, and its lattice spacing after testing is 0.24 nm (Figure S11b), thus demonstrating a stable composite structure. In addition, PdPb-Pb$(OH)_2$ composites almost can maintain its initial EOR activity compared to commercial Pd/C (Figure 3e). This result may be explained by the fact that the incorporation of Pb species and strong synergistic effect between amorphous Pb$(OH)_2$ and bimetallic PdPb alloys contribute to the outstanding EOR performance.

According to the previous works, Pd-based electrocatalysts are more susceptible to poisoning by chemisorbed intermediates (especially CO), which may block the active sites and prevent further oxidation of ethanol.[27] To investigate the mechanism of CO tolerance on PdPb-Pb$(OH)_2$, CO stripping and a series of CO poisoning measurements were employed in the alkaline medium.[28] As shown in Figure 4a, a sharp oxidation peak can be observed in the first scan on the commercial Pd/C in the potential range of −0.3 to −0.1 V, while no oxidation peak appears in the second scan, indicating that CO_{ad} on the Pd/C surface is completely removed. For PdPb-Pb$(OH)_2$ composites (Figure 4b), a very weak oxidation peak can be observed at about −0.2 V, which can be attributed to the oxidation of CO_{ad}. The initial oxidation potential has a negative shift of 0.2 V compared to Pd/C, indicating that amorphous Pb$(OH)_2$ can accelerate the removal of CO_{ad}.[29] Based on the above results, it can be concluded that the incorporation of Pb species can optimize the Pd−Pd interatomic distance and adjust the d-band center of Pd, thus leading to enhanced CO tolerance. Importantly, amorphous Pb$(OH)_2$ species may also involve in promoting the formation of OH_{ad} species adjacent to the Pd active sites. This is because amorphous Pb$(OH)_2$ species with rich crystal defects could greatly accelerate the dissociation of H_2O to generate more OH_{ad}. The interaction between amorphous metal hydroxides and OH_{ad} species is neither too strong nor too weak, which favors the oxidative removal of CO_{ad} ($CO_{ad} + OH_{ad} \rightarrow CO_2 + H^+ + e^-$).[30,31] Therefore, the strong synergistic effect between amorphous Pb$(OH)_2$ and bimetallic PdPb alloys can be attributed to the formation of OH_{ad} species adjacent to the Pd active sites, resulting in promoting the oxidative removal of CO_{ad}.

CO poisoning experiments were performed to further demonstrate the key role of Pb$(OH)_2$ species. Compared to the CV curves recorded in the N_2-saturated 1 M NaOH + 1 M ethanol solution, the current density of Pd/C decreases to 0.74 A mg_{Pd}^{-1} in the CO-saturated 1 M NaOH + 1 M ethanol solution (Figure 4c). In contrast, PdPb-Pb$(OH)_2$ composites can remain similar EOR activity, demonstrating their greater CO tolerance (Figure 4d). Importantly, when CO gas was bubbled into the electrolytes at 200 s during the CA test, the current density of Pd/C immediately drops to zero, while the current density of PdPb-Pb$(OH)_2$ composites has a typical peak and then keeps its beginning trend, further verifying the superior CO tolerance (Figure 4e,f). Based on the above discussion, the incorporation of amorphous Pb$(OH)_2$ contributes to the strong synergistic effect with bimetallic PdPb alloys, which is beneficial to the enhancement of antipoisoning ability.

4. CONCLUSIONS

In summary, bimetallic PdPb nanocrystals with the modification of amorphous Pb$(OH)_2$ have been prepared via a solution-phase chemical method. Taking advantage of the tuned electronic structure of Pd by the incorporation of Pb species, PdPb-Pb$(OH)_2$ composites show better EOR performance compared to commercial Pd/C. More importantly, the surface modification of amorphous Pb$(OH)_2$ can greatly promote the oxidative removal of CO intermediate by accelerating the formation of OH_{ad} adjacent to the Pd active sites, leading to the superior EOR durability. This work highlights the importance of the composite construction between Pd and Pb$(OH)_2$ species for the enhanced EOR performance.

■ ASSOCIATED CONTENT

Supporting Information

The Supporting Information is available free of charge at https://pubs.acs.org/doi/10.1021/acsomega.2c03693.

Additional characterizations; additional SEM images; and additional electrocatalytic testing curves: Figures S1−S11 and Table S1 (PDF)

■ AUTHOR INFORMATION

Corresponding Authors

Yuan Liu − *School of Chemistry and Chemical Engineering, Nantong University, Nantong 226019, China*; Email: liuyuan1105@ntu.edu.cn

Ping Hua − *School of Chemistry and Chemical Engineering, Nantong University, Nantong 226019, China*; Email: hua.p@ntu.edu.cn

Xiaolei Yuan − *School of Chemistry and Chemical Engineering, Nantong University, Nantong 226019, China*; orcid.org/0000-0002-8660-7246; Email: xlyuan@ntu.edu.cn

Authors

Jialu Huang − *School of Chemistry and Chemical Engineering, Nantong University, Nantong 226019, China*

Zhiming Ni − *Sales Department, Petrochina Tuha Oilfield Company, Turpan 838200 Xinjiang, China*

Xiaofan Song − *State Key Laboratory of Space Power-Sources Technology, Shanghai Institute of Space Power-Sources, Shanghai 200245, China*

Han Li − *School of Chemistry and Chemical Engineering, Nantong University, Nantong 226019, China*

Xiaolei Chen − *School of Chemistry and Chemical Engineering, Nantong University, Nantong 226019, China*

Aichuang Zhang − *School of Chemistry and Chemical Engineering, Nantong University, Nantong 226019, China*

Hu Yang − *School of Chemistry and Chemical Engineering, Nantong University, Nantong 226019, China*

Peng Zhu − *School of Chemistry and Chemical Engineering, Nantong University, Nantong 226019, China*

Complete contact information is available at: https://pubs.acs.org/10.1021/acsomega.2c03693

Author Contributions

This manuscript was written through contributions of all authors. All authors have given approval to the final version of the manuscript

https://doi.org/10.1021/acsomega.2c03693
ACS Omega 2022, 7, 35720−35726

Notes

The authors declare no competing financial interest.

■ ACKNOWLEDGMENTS

This work was supported by the Natural Science Foundation of Jiangsu Province (BK20200960), the Natural Science Foundation of Higher Education in Jiangsu Province (20KJB150041), and the Natural Science Foundation of Nantong University for High-Level Talent (03083033).

■ REFERENCES

(1) Yang, F.; Ye, J.; Yuan, Q.; Yang, X.; Xie, Z.; Zhao, F.; Zhou, Z.; Gu, L.; Wang, X. Ultrasmall Pd-Cu-Pt Trimetallic Twin Icosahedrons Boost the Electrocatalytic Performance of Glycerol Oxidation at the Operating Temperature of Fuel Cells. *Adv. Funct. Mater.* **2020**, *30*, No. 1908235.

(2) Wang, C.; Li, C.; Liu, J.; Guo, C. Engineering Transition Metal-Based Nanomaterials for High-Performance Electrocatalysis. *Mater. Rep.: Energy* **2021**, *1*, No. 100006.

(3) Yang, X.; Yao, K.; Ye, J. Y.; Yuan, Q.; Zhao, F.; Li, Y.; Zhou, Z. Interface-Rich Three-Dimensional Au-Doped PtBi Intermetallics as Highly Effective Anode Catalysts for Application in Alkaline Ethylene Glycol Fuel Cells. *Adv. Funct. Mater.* **2021**, *31*, No. 2103671.

(4) Zhao, F.; Yuan, Q.; Luo, B.; Li, C.; Yang, F.; Yang, X.; Zhou, Z. Surface Composition-Tunable Octahedral PtCu Nanoalloys Advance the Electrocatalytic Performance on Methanol and Ethanol Oxidation. *Sci. China Mater.* **2019**, *62*, 1877−1887.

(5) Chen, L.; Lu, L.; Zhu, H.; Chen, Y.; Huang, Y.; Li, Y.; Wang, L. Improved Ethanol Electrooxidation Performance by Shortening Pd−Ni Active Site Distance in Pd−Ni−P Nanocatalysts. *Nat. Commun.* **2017**, *8*, No. 14136.

(6) Li, C.; Yuan, Q.; Ni, B.; He, T.; Zhang, S.; Long, Y.; Gu, L.; Wang, X. Dendritic Defect-Rich Palladium−Copper−Cobalt Nanoalloys as Robust Multifunctional Non-Platinum Electrocatalysts for Fuel Cells. *Nat. Commun.* **2018**, *9*, No. 3702.

(7) Lv, H.; Wang, Y.; Lopes, A.; Xu, D.; Liu, B. Ultrathin PdAg Single-Crystalline Nanowires Enhance Ethanol Oxidation Electrocatalysis. *Appl. Catal., B* **2019**, *249*, 116−125.

(8) Wang, H.; Jiao, L.; Zheng, L.; Fang, Q.; Qin, Y.; Luo, X.; Wei, X.; Hu, L.; Gu, W.; Wen, J.; Zhu, C. PdBi Single-Atom Alloy Aerogels for Efficient Ethanol Oxidation. *Adv. Funct. Mater.* **2021**, *31*, No. 2103465.

(9) Miao, B.; Wu, Z.-P.; Zhang, M.; Chen, Y.; Wang, L. Role of Ni in Bimetallic PdNi Catalysts for Ethanol Oxidation Reaction. *J. Phys. Chem. C* **2018**, *122*, 22448−22459.

(10) Wu, P.; Huang, Y.; Zhou, L.; Wang, Y.; Bu, Y.; Yao, J. Nitrogen-Doped Graphene Supported Highly Dispersed Palladium-Lead Nanoparticles for Synergetic Enhancement of Ethanol Electrooxidation in Alkaline Medium. *Electrochim. Acta* **2015**, *152*, 68−74.

(11) Ma, N.; Wang, S.; Liu, X.; Sun, Y.; Yin, Y.; Zhang, L. Y.; Guo, P. PdPb Bimetallic Nanowires as Electrocatalysts for Enhanced Ethanol Electrooxidation. *Sci. China Mater.* **2020**, *63*, 2040−2049.

(12) Yu, X.; Luo, Z.; Zhang, T.; Tang, P.; Li, J.; Wang, X.; Llorca, J.; Arbiol, J.; Liu, J.; Cabot, A. Stability of Pd_3Pb Nanocubes during Electrocatalytic Ethanol Oxidation. *Chem. Mater.* **2020**, *32*, 2044−2052.

(13) Huang, W.; Ma, X.-Y.; Wang, H.; Feng, R.; Zhou, J.; Duchesne, P. N.; Zhang, P.; Chen, F.; Han, N.; Zhao, F.; Zhou, J.; Cai, W.-B.; Li, Y. Promoting Effect of $Ni(OH)_2$ on Palladium Nanocrystals Leads to Greatly Improved Operation Durability for Electrocatalytic Ethanol Oxidation in Alkaline Solution. *Adv. Mater.* **2017**, *29*, No. 1703057.

(14) Yuan, X.; Zhang, Y.; Cao, M.; Zhou, T.; Jiang, X.; Chen, J.; Lyu, F.; Xu, Y.; Luo, J.; Zhang, Q.; Yin, Y. $Bi(OH)_3$/PdBi Composite Nanochains as Highly Active and Durable Electrocatalysts for Ethanol Oxidation. *Nano Lett.* **2019**, *19*, 4752−4759.

(15) Chu, M.; Huang, J.; Gong, J.; Qu, Y.; Chen, G.; Yang, H.; Wang, X.; Zhong, Q.; Deng, C.; Cao, M.; Chen, J.; Yuan, X.; Zhang, Q. Synergistic Combination of Pd Nanosheets and Porous $Bi(OH)_3$ Boosts Activity and Durability for Ethanol Oxidation Reaction. *Nano Res.* **2022**, *15*, 3920−3926.

(16) Huang, J.; Deng, C.; Liu, Y.; Han, T.; Ji, F.; Zhang, Y.; Lu, H.; Hua, P.; Zhang, B.; Qian, T.; Yuan, X.; Yang, Y.; Yao, Y. Bifunctional Effect of $Bi(OH)_3$ on the PdBi Surface as Interfacial Brønsted Base Enables Ethanol Electro-Oxidization. *J. Colloid Interface Sci.* **2022**, *611*, 327−335.

(17) Ding, Y.; Fan, F.; Tian, Z.; Wang, Z. L. Atomic Structure of Au−Pd Bimetallic Alloyed Nanoparticles. *J. Am. Chem. Soc.* **2010**, *132*, 12480−12486.

(18) Troutman, J. P.; Li, H.; Haddix, A. M.; Kienzle, B. A.; Henkelman, G.; Humphrey, S. M.; Werth, C. J. PdAg Alloy Nanocatalysts: Toward Economically Viable Nitrite Reduction in Drinking Water. *ACS Catal.* **2020**, *10*, 7979−7989.

(19) Wang, Z.; Wang, H.; Zhang, Z.; Yang, G.; He, T.; Yin, Y.; Jin, M. Synthesis of Pd Nanoframes by Excavating Solid Nanocrystals for Enhanced Catalytic Properties. *ACS Nano* **2017**, *11*, 163−170.

(20) Duan, H.; You, R.; Xu, S.; Li, Z.; Qian, K.; Cao, T.; Huang, W.; Bao, X. Pentacoordinated Al^{3+}-Stabilized Active Pd Structures on Al_2O_3-Coated Palladium Catalysts for Methane Combustion. *Angew. Chem., Int. Ed.* **2019**, *58*, 12043−12048.

(21) Li, C.; Tang, B.; Ogunbiyi, A. T.; Tang, S.; Li, W.; Lu, Q.; Yuan, L. The Effects of Facet-Dependent Palladium-Titania Interactions on the Activity of Pd/Rutile Catalysts for Lean Methane Oxidation. *Mol. Catal.* **2022**, *528*, No. 112475.

(22) Chen, L.; Zhou, L.; Lu, H.; Zhou, Y.; Huang, J.; Wang, J.; Wang, Y.; Yuan, X.; Yao, Y. Shape-Controlled Synthesis of Planar PtPb Nanoplates for Highly Efficient Methanol Electro-Oxidation Reaction. *Chem. Commun.* **2020**, *56*, 9138−9141.

(23) Zhang, Y.; Yuan, X.-L.; Lyu, F.-L.; Wang, X.-C.; Jiang, X.-J.; Cao, M.-H.; Zhang, Q. Facile One-Step Synthesis of PdPb Nanochains for High-Performance Electrocatalytic Ethanol Oxidation. *Rare Met.* **2020**, *39*, 792−799.

(24) Li, X.; Li, P.; Wu, Z.; Luo, D.; Yu, H. Y.; Lu, Z. H. Review and Perspective of Materials for Flexible Solar Cells. *Mater. Rep.: Energy* **2021**, *1*, No. 100001.

(25) Huang, Y.; Guo, Y.; Wang, Y.; Yao, J. Synthesis and Performance of a Novel PdCuPb/C Nanocatalyst for Ethanol Electrooxidation in Alkaline Medium. *Int. J. Hydrogen Energy* **2014**, *39*, 4274−4281.

(26) Jana, R.; Subbarao, U.; Peter, S. C. Ultrafast Synthesis of Flower-like Ordered Pd3Pb Nanocrystals with Superior Electrocatalytic Activities towards Oxidation of Formic Acid and Ethanol. *J. Power Sources* **2016**, *301*, 160−169.

(27) Luo, L.; Fu, C.; Yang, F.; Li, X.; Jiang, F.; Guo, Y.; Zhu, F.; Yang, L.; Shen, S.; Zhang, J. Composition-Graded Cu−Pd Nanospheres with Ir-Doped Surfaces on N-Doped Porous Graphene for Highly Efficient Ethanol Electro-Oxidation in Alkaline Media. *ACS Catal.* **2020**, *10*, 1171−1184.

(28) Vidaković, T.; Christov, M.; Sundmacher, K. The Use of CO Stripping for in Situ Fuel Cell Catalyst Characterization. *Electrochim. Acta* **2007**, *52*, 5606−5613.

(29) Yuan, X.; Jiang, B.; Cao, M.; Zhang, C.; Liu, X.; Zhang, Q.; Lyu, F.; Gu, L.; Zhang, Q. Porous Pt Nanoframes Decorated with Bi(OH)3 as Highly Efficient and Stable Electrocatalyst for Ethanol Oxidation Reaction. *Nano Res.* **2020**, *13*, 265−272.

(30) Du, W.; Yang, G.; Wong, E.; Deskins, N. A.; Frenkel, A. I.; Su, D.; Teng, X. Platinum-Tin Oxide Core−Shell Catalysts for Efficient Electro-Oxidation of Ethanol. *J. Am. Chem. Soc.* **2014**, *136*, 10862−10865.

(31) Nikoshvili, L. Z.; Bykov, A. V.; Khudyakova, T. E.; LaGrange, T.; Héroguel, F.; Luterbacher, J. S.; Matveeva, V. G.; Sulman, E. M.; Dyson, P. J.; Kiwi-Minsker, L. Promotion Effect of Alkali Metal Hydroxides on Polymer-Stabilized Pd Nanoparticles for Selective Hydrogenation of C−C Triple Bonds in Alkynols. *Ind. Eng. Chem. Res.* **2017**, *56*, 13219−13227.

https://doi.org/10.1021/acsomega.2c03693
ACS Omega 2022, 7, 35720−35726